arXiv:astro-ph/0112470v1 20 Dec 2001

Bull. Astr. Soc. India (0000) **00**, 000–000

MSX Observations of Diffuse UV Emission in Orion

Jayant Murthy,[1*] R. C. Henry[2], L. J. Paxton[3] and S. D. Price[4]
[1] *Indian Institute for Astronomy, Koramangala, Bangalore 560 034*
[2] *Department of Physics and Astronomy, The Johns Hopkins University, Baltimore, MD 21218*
[3] *The Johns Hopkins University Applied Physics Laboratory. Laurel, MD 20723*
[4] *AFRL Hanscomb AFB, MA 01731*

2008 February 1

Abstract. We have observed intense diffuse radiation in the UV (1400 Å - 2600 Å) from three fields around M42 in Orion. Intensities of 20000 photons cm^{-2} sr^{-1} s^{-1} $Å^{-1}$ were observed to the east and west of M42 with 8000 photons cm^{-2} sr^{-1} s^{-1} $Å^{-1}$ south of the nebula. Enhanced emission, perhaps associated with a nearby complex of molecular clouds observed in CO, was detected in one of the fields. The *IRAS* 100 μm emission in that region is highly correlated with the UV intensity with a UV-IR ratio of 40 photons cm^{-2} sr^{-1} s^{-1} $Å^{-1}$(MJy $sr^{-1})^{-1}$. In the other two fields there was no structure in the diffuse emission nor was there any correlation with the *IRAS* emission.

Keywords : reflection nebulae; Ultraviolet: ISM - ISM: clouds - dust, extinction

1. Introduction

The *Midcourse Space Experiment* (*MSX*) was a US Ballistic Missile Defense Organization (BMDO) satellite launched on 26 April 1996, from Vandenberg AFB into a 900 km altitude, semi-sun synchronous orbit. Mill et al. (1994) provide an overview of the *MSX* mission and objectives, which included observations of a variety of natural and man-made phenomena over a spectral range from the ultraviolet to the mid-infrared.

*e-mail: jmurthy@yahoo.com

A large number of astronomical observations were made during the mission, characterizing various components of celestial backgrounds. Price et al. (1997) describe the objectives of the 11 *MSX* astronomy experiments, designated "CB" (for Celestial Background), and also detail the data obtained by SPIRIT III, the infrared telescope aboard *MSX*. The ultraviolet and visible sensor suite of four imagers and five hyperspectral imagers (collectively called UVISI) on *MSX* are described by Hefferman et al. (1996) and Paxton et al. (1996).

In the first part of the mission (May, 1996 to February, 1997), the infrared instruments had the highest priority and were used to scan many interesting regions of the sky. Although the two UV imagers and five hyperspectral imagers (SPIMs) did take data during this phase, while the IR measurements were being made, it was only after the cryogen ran out (February 1997) that the full suite of UVISI sensors were used to begin a systematic survey of the sky as well as dedicated observations of specific regions. More than 400 observations (covering a substantial fraction of the sky) were obtained by the end of this phase of the mission in December 1997. These experiments were denoted as CB-10 (a systematic survey of the sky) and CB-11 (observations of specific celestial targets).

The Orion nebula has long been known to be one of the brightest regions of diffuse UV emission in the sky since the first (and only) observations from a sounding rocket flight by Carruthers and Opal (1977). Despite considerable internal (instrumental) scattering, they detected a diffuse signal amounting to approximately 10% of the direct starlight, which they attributed to the scattering of starlight from interstellar dust in Orion.

In the present paper, we describe the three *MSX* observations, or "data collection events" (referred to as DCEs hereafter), in which the UVISI sensors were directed toward various regions in Orion. We detected intense UV emission in all three fields. In the following sections we describe our observations and results.

2. Observations

Because the 9 UVISI instruments were designed to observe a variety of phenomena, from ballistic missiles in midcourse to the faint diffuse astronomical radiation, a plethora of filters and operating modes were available. We list those used in our observations in Table 1. In the cryogen phase, when SPIRIT III was operational, the bandwidth available for the UVISI instruments was limited such that we were only able to download the data from one imager at a time. However, we could power two (or more) imagers and download the data from each alternately. In our cryogen phase observations, we routinely used both the narrow and wide field UV imagers. with half of the total exposure time in each. The SPIMs took much less bandwidth and we were able to operate all 5 even in the cryogen phase, albeit at a reduced spectral and spatial resolution. There were no

Table 1. UVISI Instruments

Instr.	Bandpass[a]	Field of View[b]	Res.[c]
IUW	1240 - 1380 Å (Filter 3)	$13.^{\circ}1 \times 10.^{\circ}3$	$3'$
	1430 – 1760 Å (Filter 6)		
IVW	4000 - 8500 Å (Filter 3)	$13.^{\circ}1 \times 10.^{\circ}3$	$3'$
IUN	2000 - 2500 Å (Filter 3)	$1.^{\circ}5 \times 1.^{\circ}2$	$20''$
	2000 - 2670 Å (Filter 4)		
	2230 - 2710 Å (Filter 5)		
IVN	2900 – 8270 Å	$1.^{\circ}5 \times 1.^{\circ}2$	$20''$
	Spectrographic Imagers (SPIMs)		
SPIM1	1350 - 1740 Å	$1^{\circ} \times 0.^{\circ}05$	6 Å
SPIM2	1640 - 2530 Å	$1^{\circ} \times 0.^{\circ}1$	7 Å
SPIM3	2520 - 3910 Å	$1^{\circ} \times 0.^{\circ}1$	19 Å
SPIM4	3790 - 5850 Å	$1^{\circ} \times 0.^{\circ}1$	31 Å
SPIM5	5810 - 8970 Å	$1^{\circ} \times 0.^{\circ}1$	40 Å

[a] The bandpass for the imagers was selectable using a variety of filters; we have listed only those used in our observations.

[b] The field of view for the SPIMs was selectable; only those options that were used in our observations are listed here. In all of our observations the SPIMs were operated with a spatial scan mirror, resulting in an effective field of view of $1^{\circ} \times 1.^{\circ}$ SPIM 1 included a BaF_2 filter to block the atmospheric HI and OI lines.

[c] The listed resolutions are spatial resolutions for the imagers and spectral resolutions for the SPIMs. In the cryogen phase the spectral resolution of the SPIMs was half that listed because of binning forced upon us by data bandwidth restrictions.

bandwidth restrictions in the post-cryogen phase and we operated all 9 instruments at their full resolutions.

All the UVISI instruments used essentially identical detectors — intensified CCDs — with different photocathodes. Incoming light ejected electrons from the photocathode which were amplified by a micro-channel plate to strike a green phosphor coupled by a reducing fiber optic taper to the CCD. The gain of the MCP was adjustable over a dynamic range of 10^9; however, because we were interested in observations of relatively faint astronomical sources, we normally operated at a gain high enough that individual photons could be detected well over the background. The dynamic range *within* a scene was more limited and we could not always use the photon counting mode because of bright stars in the field of view. In particular, this was the case for the wide field imagers in the Orion observations.

The CCDs were read every half second (with an integration time of 467 milliseconds) and the data were dumped to an on-board tape recorder. This rapid readout resulted

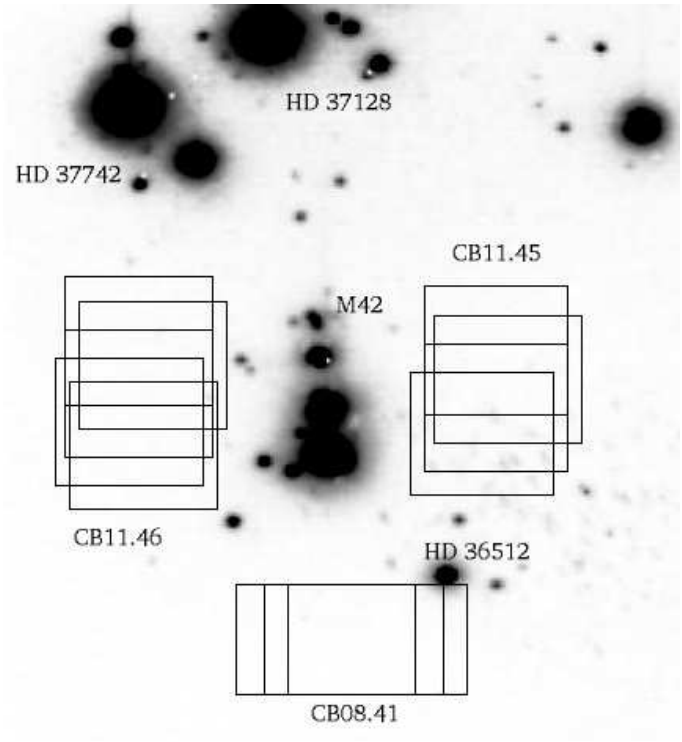

Figure 1. The positions of the 3 Orion Data Collection Events (DCES) are shown on an IUW ($13.^\circ1 \times 10.^\circ3$) image (with North at the top), with a few of the brighter stars identified: HD 37742 (ζ Ori) and HD 37128 (ϵ Ori) form part of the Orion belt. There were several pointings within each DCE, with various filters; the IUN field in each pointing is shown by a small box ($1.^\circ5 \times 1.^\circ2$). The SPIMs scanned over essentially the same field as the narrow field imagers, but with much less sensitivity. Not all of the instruments and pointings provided useful scientific data (for our purposes), for instance the IUW image shown was taken at too low a gain to allow us to detect the diffuse background.

in an enormous amount of data, typically 1 GB per data collection event (DCE). These data were processed at the Applied Physics Laboratory of the Johns Hopkins University under the supervision of the DCATT (Data Certification and Technology Transfer) team, whose responsibility it was to certify the process and the data. The starting point for our scientific analysis was "Level 1CA" data: CCD images with a distortion correction, flat fielding and calibration already applied.

We observed three regions in Orion, one in the cryogen phase and the other two after the SPIRIT III instrument was turned off. These observations are denoted, in temporal order:

CB08-41 (UJ_CB08010004101_05_9999B),

CB11-45 (UJ_CB11010004501_05_9999A), and

CB11-46 (UJ_CB11010004601_05_9999B)

and are superimposed on an IUW image of Orion in Fig. 1. In each DCE, we observed a specific location for 10 minutes and then offset the pointing by about $0.^{\circ}25$. This was repeated for a total of four pointings per DCE (three for CB08-41) with significant field overlap. In each of the two later observations (CB11-45 and CB11-46) filter changes were made after each pointing. The SPIMs used a scanning mirror to observe a $1^{\circ} \times 1^{\circ}$ field centered on the instrument boresight, overlapping much of the IUN field of view.

Although the 0.5 second integration time of the UVISI sensors resulted in an enormous amount of data, the large number of samples in a single DCE were invaluable for diagnostic information. As an illustrative example, we have plotted (Fig. 2) the total signal per frame from the narrow field of view imager (IUN) in CB11-45. At the beginning and end of each DCE and at every filter change the gain on the MCP was set to the minimum value and the observed count rate dropped to the CCD read noise, setting a floor for the observed signal (square wells in Fig. 2). The read noise was parametrized and subtracted from the data and the residual was thresholded to leave only individual photon hits (lower curve in Fig. 2). A few cosmic ray hits were bright enough to light up the entire detector and were easily identified (spikes in Fig. 2). In such a case the entire frame was discarded. Less intense events were also present and were removed by comparing the signal over several frames.

In addition, there was a general increase in the background level between frames 3200 and 4200 in all 9 instruments and persisting even through a filter closure and while the spacecraft was in an inertial hold. Similar increases in the total signal have occurred in other DCEs and, in particular, CB11-46 (executed on the following day) showed a rise at the same geographical position over central Africa. In other DCEs, the rise was over other regions of the Earth, typically at low geographical latitudes and often far from the South Atlantic Anomaly. Although we have been unable to identify the source of the signal, it is clearly terrestrial in origin and we have discarded all affected frames.

At this point, we were left with a series of frames containing the astrophysical signal plus an instrumental dark noise. These frames were added together to form a single FITS file for each instrument and for each pointing. The data product from the imagers was an image of the region observed and from the SPIMs it was a 3-dimensional file with 2 spatial dimensions and one spectral.

The dark noise in the imagers (at the operational gain) was only read at the beginning and end of the DCEs (for about a minute each) and these values are tabulated in Table 2. (Note that in CB11-45 and CB11-46 there actually was another measurement in the middle of the DCE which was compromised by the general increase in the background

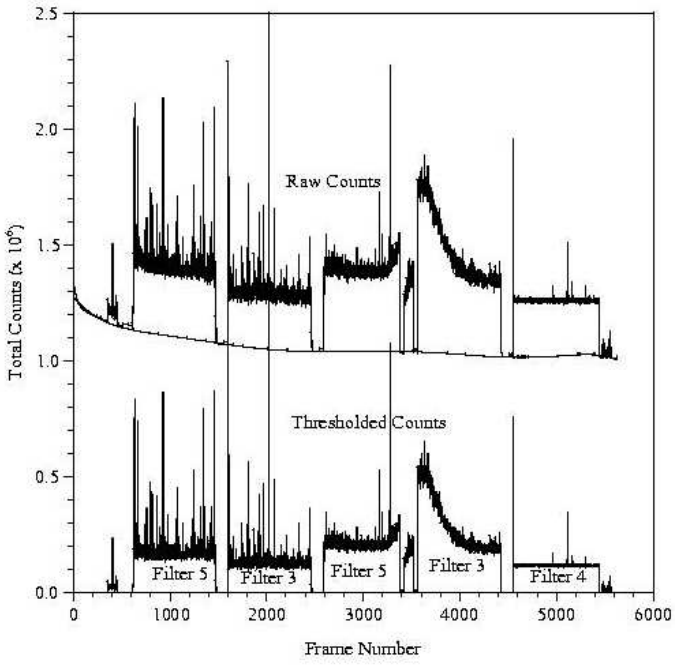

Figure 2. The count rate for the narrow field of view UV imager (IUN) in CB11-45 as a function of frame number is shown. The top line is the raw counts from the imager. From this, we have subtracted the CCD read noise (solid line) and thresholded to leave only "true" photon events (bottom line). The first 600 frames (5 minutes) were used to measure the dark current at different gains after which a series of observations were made using the indicated filters. The spikes in the data are due to bursts of noise in the CCD and were discarded. Note the big rise in the observed counts from about frame 3200 to frame 4200, persisting even through a filter closure. Such features are present in many of our DCEs and show up in all 9 instruments. We must attribute these to an undetermined terrestrial source. The last part of the observation (through Filter 4) was at a lower gain due to the presence of a bright star in the field of view. The noise from the photocathode is measured at the beginning, middle and end of each observation; in this particular DCE the middle measurement was compromised by the general rise in counts.

level already discussed.) We have used the mean of these two values as the effective dark current throughout the observation. The deviation between the two values was added in quadrature to the other errors to yield a total uncertainty. In all cases the measured dark current was much less than the observed signal.

Because there were far fewer SPIM pixels and because there were no intermediate points for the CCD read noise parametrization, the background definition in the SPIMs is very uncertain. Fortunately, SPIM 1 included a barium fluoride (BaF_2) filter which cut off all light below 1350 Å, allowing an absolute measurement of the effective background

Table 2. Dark Current

	counts pixel^{-1} s^{-1}	Effective Flux[a]
CB08-41 (start)	0.0096	1700
CB08-41 (end)	0.0034	600
CB11-45 (start)	0.025	4400
CB11-45 (end)	0.010	1750
CB11-46 (start)	0.025	4400
CB11-46 (end)	0.023	4000

[a]photons cm^{-2} sr^{-1} s^{-1} Å^{-1} This column contains the dark count converted into an effective photon flux (using the same calibration as was used for the data).

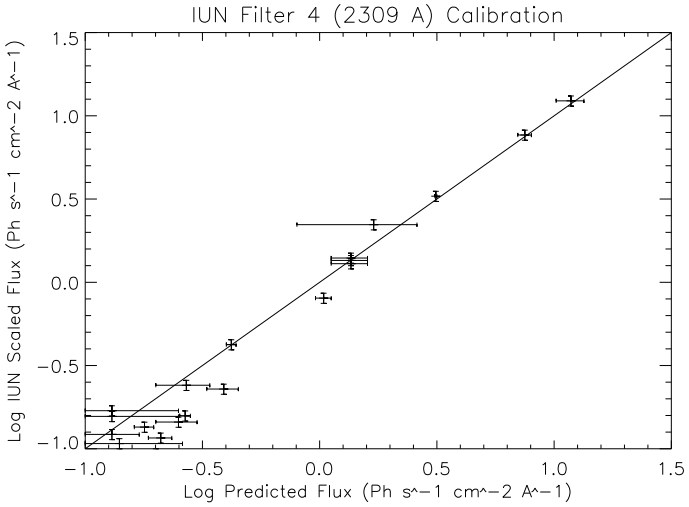

Figure 3. The flux observed by IUN filter 4 is compared with predicted fluxes using spectral types from the SIMBAD database scaled to the flux observed by TD-1. The observed fluxes match the predicted fluxes over a wide range of brightnesses. We note that these data were taken from a random sample of fields observed throughout the mission.

level. There was some wavelength overlap between the different SPIMs and we could estimate the background subtraction in the other SPIMs by forcing the spectra to be continuous. However, in practice, because of the uncertainties in matching the continua and the cumulative errors in the longer wavelength SPIMs, we could only obtain useful results for SPIMs 1 and 2, the two UV SPIMs.

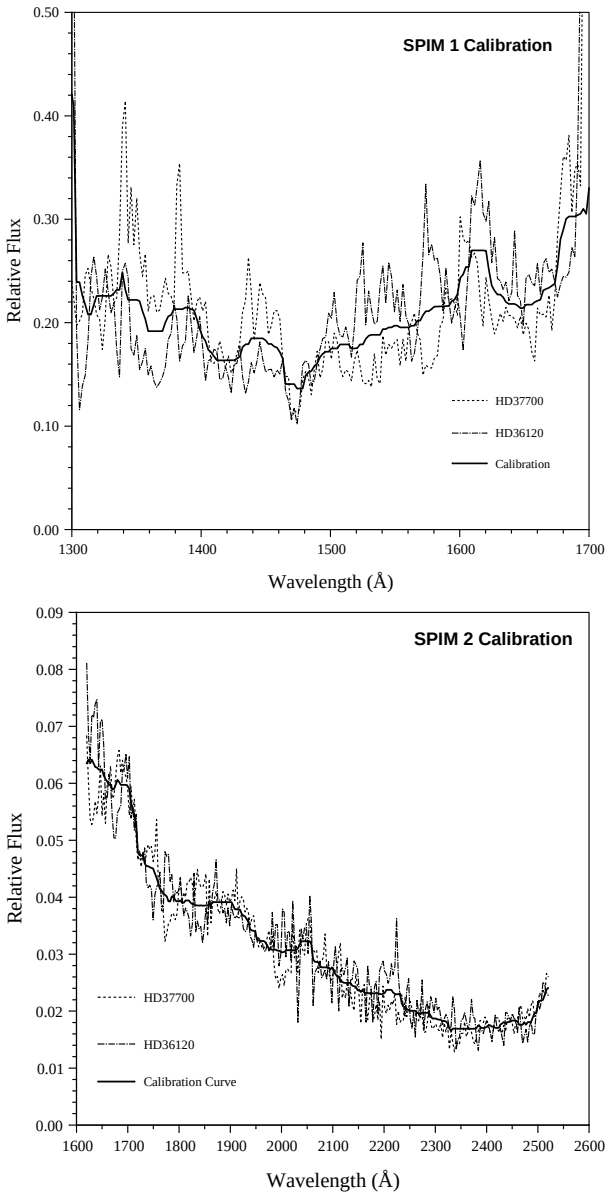

Figure 4. The ratios between the observed SPIM fluxes and the calibrated stellar fluxes as observed by IUE are plotted for two different stars. Note the generally excellent agreement between the calibration curves derived from the two stars. We adopted the median filtered average of the two curves as our calibration curve. Note that because of background subtraction problems we only calibrated the two shortest wavelength SPIMs (SPIMs 1 and 2).

Table 3. Diffuse Radiation in Two Fields

	Flux[a]
CB08-41 (Filter 4)	7400 ± 900
CB08-41 (Filter 4)	7700 ± 900
CB08-41 (Filter 4)	7300 ± 800
CB11-45 (Filter 3)	16000 ± 6000
CB11-45 (Filter 5)	20000 ± 5000

[a]photons cm^{-2} sr^{-1} s^{-1} Å^{-1}

3. Calibration

The Data Certification and Technology Transfer (DCATT) team had primary responsibility for characterizing and calibrating the instrument. However, the calibration in the photon counting mode was dependent on the details of the processing and we evolved our own calibration procedures (Newcomer et al. 2001). We extracted stars from many different DCEs and identified them using the SIMBAD database. If, and only if, the stars had TD-1 fluxes with reliable spectral types, we calculated their brightness in each of the instruments and filters and compared with the observed brightmess. We have plotted one of these calibration curves in Fig. 3; others are shown by Newcomer et al. (2001). In each case, the calibration proved to be both linear and stable over a large range of brightnesses and over the lifetime of the satellite. Note that we were forced to reject many of the observed stars for calibration purposes because of spectral types which were clearly inconsistent with the TD-1 measurements.

The SPIM calibration is based on two stars (HD 36210 and HD 37700) for which high quality IUE spectra (both SWP and LWP) exist. We integrated the flux around each star, estimating the background from the neighbouring pixels, and compared with the archived IUE spectra. The calibration curves derived from the two stars (independently) are plotted in Fig. 4 and are entirely consistent with each other. Because our primary spectroscopic science comes from SPIMs 1 and 2, the two UV SPIMs, and because of the background subtraction problems in the longer wavelength SPIMs, we have focussed on the data from those two spectrographs in this paper.

4. Results

We observed intense diffuse ultraviolet emission in three regions around M42 in Orion at levels of more that 2×10^4 photons cm^{-2} sr^{-1} s^{-1} Å^{-1} to the east and west of M42. A lower, but still high, level of 8000 photons cm^{-2} sr^{-1} s^{-1} Å^{-1} was observed south of the nebula (CB08-41). Instrumental scattering from the many bright stars in Orion was clearly visible in a few pointings in each DCE and we have used only those parts of each

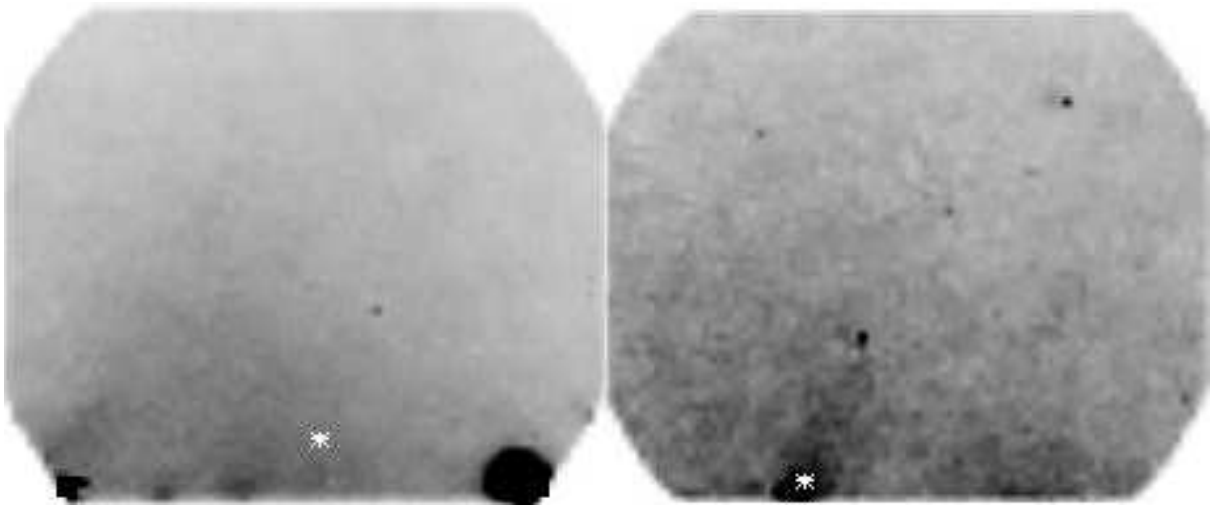

Figure 5. Images from CB11-46 are shown (North to the right and East to the top) for IUN Filter 4 (on the left) and IUN Filter 3. The asterisk is at the same coordinates in both images (RA:05 39 29.26 , Dec:-05 41 25.2). A bright patch is visible in both images and is probably an extended halo to the complex of molecular clouds identified by Ogura & Sugitani (1998) about 15' to the west (bottom) of the image.

image which were observed in multiple pointings and in which the measured flux was consistent between pointings.

In two of the DCEs — CB08-41 and CB11-45, to the south and west of M42, respectively — the flux was uniform with levels tabulated in Table 3. However, a bright patch was observed in CB11-46 (Figure 5), most likely emission from the outlying regions of the complex of molecular clouds detected by Ogura & Sugitani (1998) about 15′ away.

The UV flux is tightly correlated with the 100 μm *IRAS* emission in CB11-46 (Figure 6) with a UV-IR ratio of about 40 photons cm^{-2} sr^{-1} s^{-1} Å^{-1}/(MJy sr^{-1})$^{-1}$. The UV to IR ratio from the other two observations is quite different (also plotted in Fig. 6), particularly for CB11-45 where the UV flux does not vary at all despite a factor of 4 variation in the IRAS 100 μm flux.

The only other determination of the UV to IR ratio has come from Haikala et al (1995) who used FAUST observations of an isolated Galactic cirrus cloud to derive a ratio of 128 photons cm^{-2} sr^{-1} s^{-1} Å^{-1}(MJy sr^{-1})$^{-1}$. Although the combination of UV and IR observations of the same region can provide great insight into the optical properties of the dust grains, both the UV and the IR emission are highly dependent on the exact geometry of the stars and the dust and detailed modeling is required to deconvolve the properties and nature of the dust.

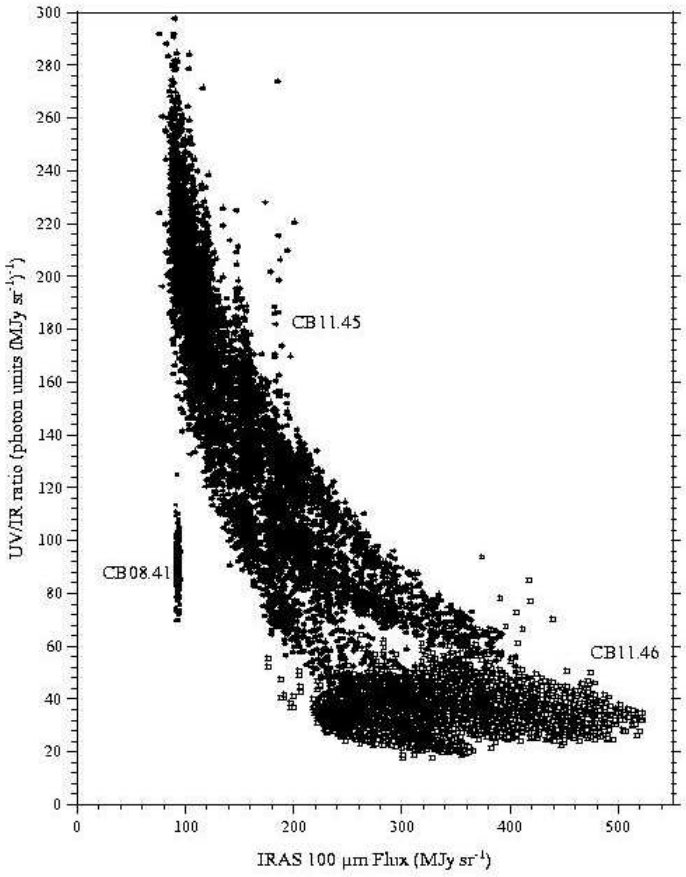

Figure 6. The correlations between the UV flux observed by IUN (photons cm^{-2} sr^{-1} s^{-1} Å^{-1}) and the IRAS 100 μm flux MJ sr^{-1}) in plotted for the three DCEs observed. In CB08-41 there is not much variation in either the IR or the UV fluxes; in CB11-45 the UV flux is almost constant while the infrared varies over a factor of 4; and in CB11-46 both vary while keeping the ratio constant.

We also obtained spatial maps of the three DCEs with SPIMs 1 and 2 (due to processing problems only SPIM 1 was available for CB08-41). There was no evidence for spatial variability in the diffuse radiation detected by the SPIMs, after discarding the data near the bright stars in the field, and so we simply integrated over the entire field of view to give the spectra plotted in Figure 7. Allowing for the different instrumental passbands, the diffuse backgrounds detected by the SPIMs are consistent with those detected by IUN. We note that, because of a drop in the gain of the SPIMs in the middle of the DCE for CB11-46, the SPIMs observed only the eastern half of the field.

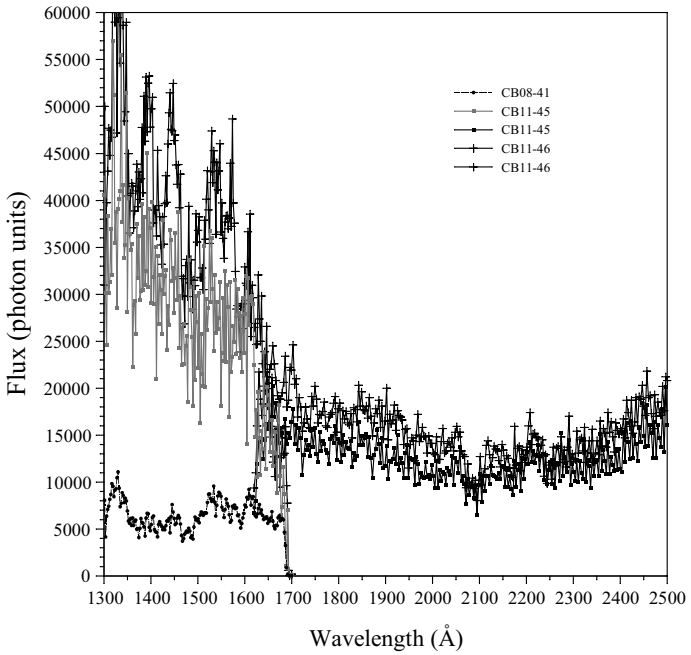

Figure 7. The spatially integrated spectra observed by the two UV SPIMs in CB11-45 and CB11-46 are plotted with the legend on the right. Due to processing problems, we could not use the SPIM 2 spectrum from CB08-41 and so only the spectrum from SPIM 1 is shown. Given the different bandpasses, the levels are consistent with the respective IUN fluxes. Note that the SPIM coverage in CB11-46 did not include the bright patch observed by IUN

5. Conclusions

We have observed intense diffuse radiation from three fields around M42 in Orion. This background is much brighter to the east and west of the nebula with intensities of more that 2 x 10^4 photons cm^{-2} sr^{-1} s^{-1} Å^{-1} dropping to 8000 photons cm^{-2} sr^{-1} s^{-1} Å^{-1} to the south of M42. In one of the DCEs (CB11-46 to the east of M42), we detected a bright patch which may be related to the nearby molecular clouds of Ogura & Sugitani (1998). In the other two regions, the emission was uniform.

The UV flux was directly correlated with the IR in CB11-46 with a ratio of about 40 photons cm^{-2} sr^{-1} s^{-1} Å^{-1} (MJy sr^{-1})$^{-1}$. No such relation was observed in CB11-45 where, despite a factor of 4 variation in the *IRAS* 100 μm flux, the UV was essentially constant over the field. The only other measurement of the UV-IR ratio was the 128 photons cm^{-2} sr^{-1} s^{-1} Å^{-1} (MJy sr^{-1})$^{-1}$ obtained by Haikala et al (1995) for an isolated Galactic cirrus cloud. It is clear, and should be expected, that the UV-IR ratio is heavily dependent on the environment.

In principle, the combination of IR and UV observations in a single direction will strongly constrain the optical properties of the dust grains. Stellar radiation penetrates into the interior of the clouds and some part is scattered in the UV. That part not scattered will be absorbed and then reemitted as thermal radiation in the IR. In practice, a detailed study is required to realistically model the penetration and subsequent reradiation of the input radiation field by the optically thick (in the UV) dust. We are beginning such a study for simple geometries where we have Voyager and IRAS data and hope, eventually, to extend it to more complex regions such as Orion.

This work was supported at the Johns Hopkins University by USAFG F19628-93-K-0004

References

Carruthers, G. R. & Opal, C. B. 1977, ApJ, 217, 96.

Haikala, L. K., Mattila, K., Bowyer, S., Sasseen, T. P., Lampton, M., & Knude, J. 1995, ApJL, 443, L33.

Heffernan, K. J., Heiss, J. E., Boldt, J. D., Darlington, E. H., Peacock, K., Harris, T. J., & Mayr, M. J. 1996, Johns Hopkins APL Technical Digest, V17, 198.

Mill, J. D., O'Neil, R. R., Price, S., Romick, G. J., Uy, O. M., Gaposchkin. E. M., Light, G. C., Moore Jr., W. W., Murdock, T. L., & Stair, A. T. 1994, Journal Spacecraft and Rockets, 31, No. 5 900.

Newcomer, R., Henry, R. C. , Murthy, J., Paxton, L. J., & Price, S. D. 2001.

Ogura, K. & Sugitani, K 1998, Publications of the Astronomical Society of Australia, 15, 91.

Paxton, L. J, Meng, C.-I., Anderson, D. E., & Romick, G. J. 1996, Johns Hopkins APL Tech. Digest, 17, 19.

Price, S. D., Tedesco, E. F. Cohen, M. Walker, R. G. Henry, R. C. Moshir, M. Paxton, L. J. and Witteborn, F. C. 1997 in "Proceedings of IAU Symposium 179, New Horizons from Multi-Wavelength Sky Surveys," ed. B. J. McLean, D. A. Golombek, J. J. E. Hayes, and H. E. Payne (Dordrecht: Kluwer), 115.

Smith, N., Egan, M. P., Carey, S., Price, S. D., Morse, J. A., & Price, P. A. 2000, ApJ, 532, 145.